Chemical State of Complex Uranium Oxides

K. O. Kvashnina,[1,*] S. M. Butorin,[2] P. Martin,[3] and P. Glatzel[1]

[1]European Synchrotron Radiation Facility, 6 Rue Jules Horowitz, BP 220, 38043, Grenoble, France
[2]Department of Physics and Astronomy, Uppsala University, Box 516, S-751 20 Uppsala, Sweden
[3]CEA, DEN, DEC, CEN Cadarache, 13108, St. Paul lez Durance, France

(Received 19 February 2013; published 17 December 2013)

We report here the first direct observation of U(V) in uranium binary oxides and analyze the gradual conversion of the U oxidation state in the mixed uranium systems. Our finding clarifies previous contradicting results and provides important input for the geological disposal of spent fuel, recycling applications, and chemistry of uranium species.

DOI: 10.1103/PhysRevLett.111.253002 PACS numbers: 31.15.X−, 28.41.Bm, 28.41.Kw

Uranium oxides are fascinating materials not only owing to their technological significance in nuclear fuel applications [1] but also with respect to their dynamical properties [2], valence orbital configuration [3], and elementary excitations [4]. Understanding of the electronic, magnetic, and crystal structural properties of uranium dioxide (UO_2) was advanced significantly [5,6] after establishing a Mott-Hubbard insulator behavior in UO_2 (see, e.g., Ref. [7]). Uranium dioxide with a fluorite type crystal structure is thermodynamically stable, but upon oxidation generates a series of the mixed-valence U oxides U_4O_9/U_3O_7 and U_3O_8 where the stochiometry depends on the temperature and oxygen partial pressure [8]. These processes are typical for the nuclear fuel cycle. UO_2 as the main component of the nuclear fuel rods is generally considered to be the safest chemical form for disposal purposes because of the low solubility of U(IV) over a wide range of environmental conditions. Uranium dioxide in contact with air can be quickly oxidized to U_3O_8 even at very low temperature ($\sim 200\,^{\circ}C$). The formation of U_3O_8 from UO_2 results furthermore in volume increase which can potentially damage the first confinement barrier (also known as fuel cladding) in the case of direct storage of fuel elements. The phase of U_3O_8 occurs as an end product not only with UO_2 as a starting material but also when other nuclear fuel sources like U dicarbides and U hydrides are used [9,10]. To avoid the risk related to the release of radionuclides to the environment during the disposal of nuclear waste [1], U_3O_8 is often recycled to spent nuclear oxide fuel [11]. Uranium oxides are not only used in power plants but also, e.g., catalysis applications. The use of U_3O_8 was encouraged in U_3O_8/SiO_2 catalysts which can efficiently destroy a range of hydrocarbons and chlorine-containing pollutants [12], because of the believed availability of two distinct oxidation states U(VI) and U(IV) and easy conversion between them [13]. In all applications a direct observation of the U chemical state is of paramount importance.

The existence of a variety of stochiometric and nonstochiometric U oxides with their complex physical and chemical properties makes them demanding systems to characterize. One of the key scientific challenges is exact determination of the oxidation states of mixed-valence U oxides, since it is the oxidation state that controls the chemical reactivity of the U ion in catalysis applications and in the environment. Recent electronic structure theoretical calculations [14] suggested that transformation of UO_2 to the U_3O_8 phase may occur through the creation of U(V) ions in the structure, but no direct experimental evidence was found to date. The lack of knowledge concerning the oxidation state triggers elaborate studies of defect sites of mixed U oxides at different temperatures and pressures by both theoretical and experimental methods [14–16]. We report here the first straightforward identification of the oxidation state changes during the gradual conversion of UO_2 to the mixed-valence U oxides. The contribution of various U oxide phases depends on the conditions of the specific reactions (temperature and pressure and reacting agent) and knowledge of the U chemical state is a prerequisite for a better understanding of the reaction paths as well as the crystallographic and thermodynamic properties.

A large body of literature has been dedicated to studies of oxygen incorporation in UO_{2+x}. Neutron and x-ray powder diffraction experiments [17–19] showed that an increase of the oxygen content involves the distortion of the UO_{2+x} crystal structure. At least 14 distinct crystallographic structures were reported for U oxides during the transformation of UO_2 to U_3O_8. One heavily debated topic was the observation of small U-O distances in the U_4O_9 compound, which are characteristic for U(VI) compounds [20]. This was questioned by other theoretical and experimental works [18,21] that assumed that U_4O_9 is a mixture of U(IV) and U(V). The U_3O_8 and U_4O_9 systems can have two possible combinations of U valences per unit cell

$$U_3O_8 = U(IV) + 2^*U(VI) \quad \text{or} \quad 2^*U(V) + U(VI),$$

$$U_4O_9 = 2^*U(IV) + 2^*U(V) \quad \text{or} \quad 3^*U(IV) + U(VI).$$

A number of studies to determine the U oxidation state for these systems have been reported using nondestructive

spectroscopic methods: x-ray photoelectron spectroscopy (XPS) [13,22], electron energy-loss spectroscopy (EELS) [23], x-ray absorption near edge structure (XANES) [20,23,24], resonant inelastic soft x-ray scattering (RIXS) [25], and laser-induced fluorescence (LIF) spectroscopy [26]. Spectroscopic techniques often use the shifts in energy position of the main absorption or emission transitions in order to determine the U valence state. An effective nuclear charge fluctuation of an atom usually results in changes of the valence electron configuration responsible for the energy shift (cf. top panel of Fig. 1). XPS does not give the opportunity for direct and unambiguous valence identification because the chemical shift of the main U $4f$ lines in the series UO_2, U_3O_8, U_4O_9, U_3O_7 is small compared to the spectral linewidth [22,27]. The analysis of XPS data therefore relies on the position of the shake-up satellite lines that arise from charge transfer excitations between the O $2p$ band and the U $5f$ level [22,27] that is induced by the photoionization process. Valence band XPS and UV photoelectron spectroscopy (UPS) measurements can provide information about the U $5f$ occupancy in the system but cannot distinguish between inequivalent U sites with different oxidation states [28,29]. Another common method is XANES spectroscopy at the U L_3 edge (~ 17.1 keV) [24,30]. The chemical shift of the main edge transitions for different U oxidation states was found to be on the order of ~ 1.0 eV between U(IV) and U(VI) systems [20,23,24]. This has to be compared to the spectral line broadening of 7.4 eV due to the short core hole life time at the U $2p_{3/2}$ level [31]. Under these conditions the detection of a U(V) signal is very difficult. Also the EELS, RIXS, and LIF studies were not conclusive and direct determination of the U oxidation states remained elusive.

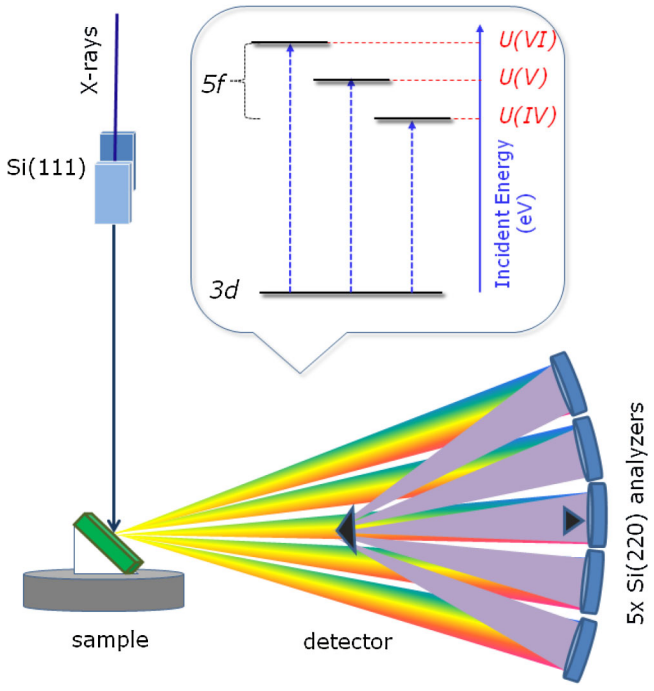

FIG. 1 (color online). Top: simplified single electron scheme of the transitions at the U M_4 edge for the different oxidation states. Bottom: schematic drawing of the x-ray emission spectrometer used during the high energy resolution fluorescence detection experiments.

According to the dipole selection rules, XANES spectra at the U L_3 ($2p_{3/2}$) edge provide information about the unoccupied U $6d$ states in the system. Most of the unique properties of U compounds, however, originate from the localized $5f$ states that can be probed at the U $M_{4,5}$ ($3d_{3/2,5/2}$) absorption edges [32,33]. The transitions at the U M edge lie in the energy range of relatively soft x rays (3.5–3.7 keV) making the experiment challenging to perform due to significant x-ray absorption by air compared to measurements at the U L_3 edge. X-ray experiments at the U M edge are also more favorable because the core hole lifetime broadening of the spectral features is smaller than at the L edge. A further reduction of the line broadening can be achieved by high energy resolution fluorescence detection (HERFD) x-ray absorption spectroscopy where an x-ray emission spectrometer (cf. Fig. 1) is employed for data collection [34]. We studied the U XANES at the M_4 edge by tuning the crystal analyzers to the maximum of the U $M\beta$ ($4f_{5/2} - 3d_{3/2}$) x-ray emission line. In the present study an experimental energy bandwidth of 0.7 eV was achieved resulting in an effective spectral broadening of 0.9 eV [35]. By employing such an experimental setup the spectral broadening matches the expected chemical shift per oxidation state and a detailed study of the U oxidation states is possible. (We note that significantly better spectral resolution can be achieved using other spectroscopic techniques. It is, however, the combination of element selectivity in inner-shell spectroscopy and good spectral resolution that enable us to unequivocally reveal the chemical state of U. The LIF data, for example, exhibit excellent spectral resolution [26] but additional features in the LIF spectra that are not associated with the U ion may not allow for an unambiguous interpretation of the results.)

The measurements were performed at beam line ID26 of the European Synchrotron Radiation Facility (ESRF) in Grenoble [36]. The incident energy was selected using the $\langle 111 \rangle$ reflection from a double Si crystal monochromator. Rejection of higher harmonics was achieved by three Si mirrors at an angle of 3.5 mrad relative to the incident beam. XANES spectra were simultaneously measured in total fluorescence yield (TFY) mode using a photodiode and in HERFD mode using an x-ray emission spectrometer [34]. The U HERFD spectra at the M_4 edge were obtained by recording the intensity of the U $M\beta$ emission line (3336.0 eV) as a function of the incident energy. The emission energy was selected using the $\langle 220 \rangle$ reflection of five spherically bent Si crystal analyzers (with 1 m bending radius) aligned at 75° Bragg angle. The paths of

the incident and emitted x rays through air were minimized in order to avoid losses in intensity due to absorption. A combined (incident convoluted with emitted) energy resolution of 0.7 eV was obtained as determined by measuring the full width at half maximum (FWHM) of the elastic peak. The polycrystalline uranyl acetylacetonate $UO_2(acac)_2$ sample was obtained commercially from International Bioanalytical Industries (Florida, USA) and prepared as a pressed pellet. The UO_2 sintered pellet (theoretical density of 98%) was thermally treated for 24 h at 1700 °C under an Ar and 5% H_2 atmosphere in order to assure its stoichiometry. X-ray diffraction results showed the fluorite type structure with a cell parameter corresponding to stoichiometric UO_2. The U_4O_9 powder was prepared by thermal treatment of a mixture of UO_2 and U_3O_8 powders. The relative mass fraction of UO_2 and U_3O_8 was chosen in order to get an average $UO_{2.23}$ composition. An air-tight closed quartz tube was filled with a powder and underwent heat treatment at 1050 °C for 30 d, after which it was cooled slowly to room temperature for another 12 h. The obtained powder had a dark color. The quality was checked [19] by x-ray diffraction and contained less than 1% U_3O_8, assuming that the U_4O_9 phase in the sample had an oxygen composition that was very close to the phase stability limit in the phase diagram. The U_3O_8 powder was obtained via isothermal annealing at 1170 °C of a sintered UO_2 pellet in dry air. The x-ray diffraction pattern showed the expected structure. For the XANES experiment, 10 mg of U_4O_9 or U_3O_8 were diluted in 200 mg of boron nitride and pressed into a pellet. To avoid any further oxidation of these two samples, after preparation, each pellet was immediately put in a sealed copper sample holder with a 5 μm Kapton window.

Figure 2(a) shows a RIXS plane measured by scanning the incident energy across the U M_4 edge at different emission energies around the U $M\beta$ emission line of UO_2. The RIXS data are shown as a contour map in a plane of incident and transferred photon energies, where the latter represents the energy difference between incident and emitted energies. A scan at the maximum of the U $M\beta$ emission line (HERFD-XANES) corresponds to a diagonal cut through the RIXS plane. Figure 2(b) shows a comparison between the conventional XANES spectrum of UO_2 at the U M_4 edge recorded in TFY mode using a photodiode, and HERFD data recorded using an x-ray emission spectrometer illustrating the dramatic improvement in spectral resolution.

The absorption spectra are characterized by a strong resonance, the so-called white line. A higher oxidation state of U results in a shift of the U white line to higher energy (Fig. 1). Figure 3 shows the HERFD spectra at the U M_4 edge of U_4O_9 and U_3O_8 compared to those of U(IV) in UO_2 and U(VI) in $UO_2(acac)_2$ as reference systems. The shape of the main absorption peak in the HERFD spectrum of UO_2 shows an asymmetric profile, which has already been

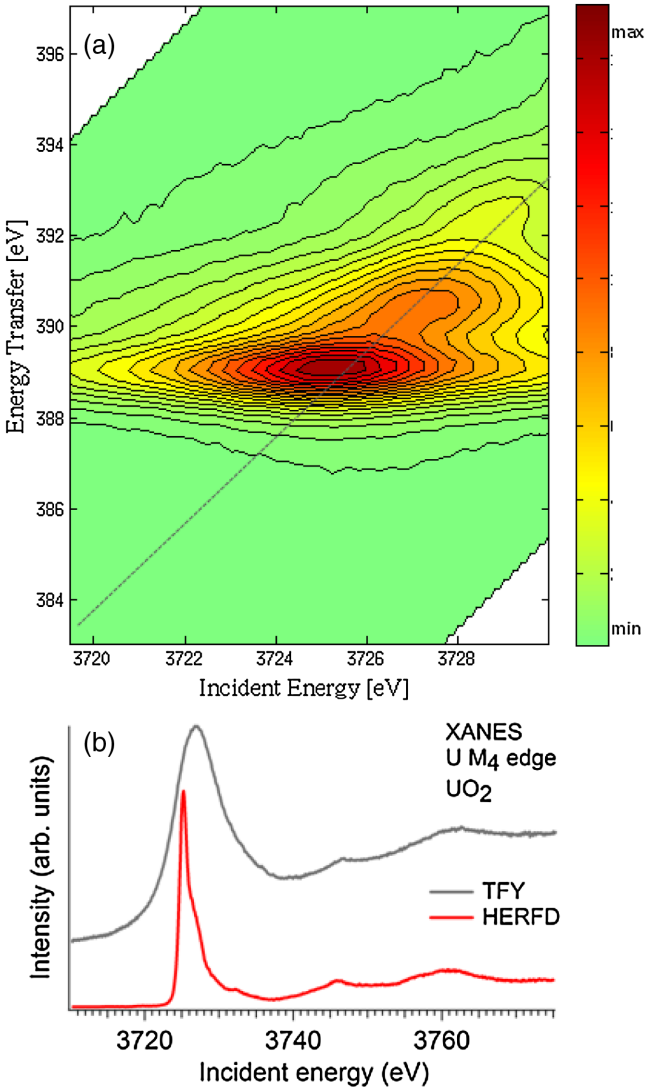

FIG. 2 (color online). (a) Experimental RIXS intensities displayed as a contour map with axes corresponding to incident and transferred energies over the U M_4 absorption edge and U $M\beta$ emission line for UO_2. Color variation in the plot relates to the different scattering intensity. A HERFD spectrum corresponds to a diagonal cut (dashed line) through the RIXS plane at the maximum of the $M\beta$ emission line. (b) HERFD at the U M_4 edge of UO_2 recorded using the x-ray emission spectrometer set to the $M\beta$ emission line (energy 3336.0 eV). The spectrum is compared to the TFY curve, recorded using a photodiode.

observed in conventional XANES experiments [32,33]. The HERFD spectrum of $UO_2(acac)_2$ shows two peaks at ~3727.0 and ~3729.0 eV. The presence of the structure at ~3729.0 eV is attributed to the characteristic feature of the uranyl ion [32,33]. The positions of the main peaks in the HERFD spectra of the reference U systems clearly reveal the energy shift of ~1.9 eV of the white line toward higher energy on going from the U(IV) to U(VI). This shift is considerably larger than what was previously observed at the U L edges [20,23,24].

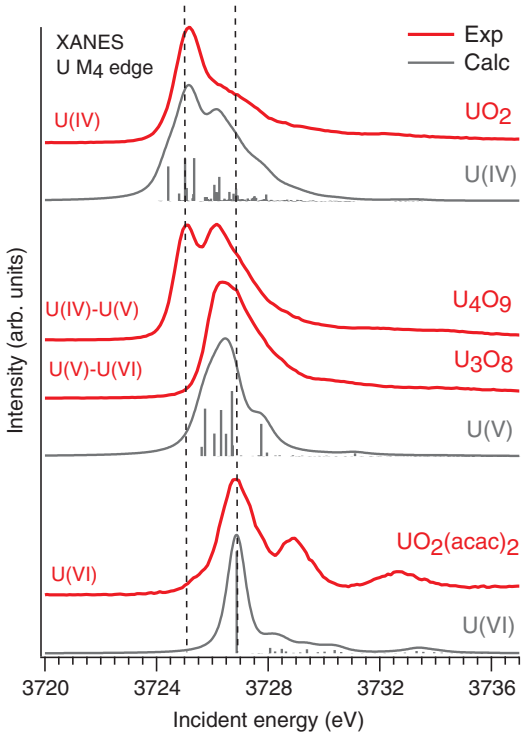

FIG. 3 (color online). HERFD-XANES experimental and calculated spectra at the U M_4 edge of U_4O_9 and U_3O_8 compared with those of reference systems UO_2 and $UO_2(acac)_2$. Dashed lines indicate the energy position of the main peaks corresponding to uranium in oxidation states IV and VI, respectively.

The width and shape of the absorption lines in U_3O_8 and U_4O_9 are very different from those in UO_2 and $UO_2(acac)_2$. Two intense peaks in the HERFD spectrum of U_4O_9 are observed. The first peak at ~3725.0 eV is associated with the U(IV) signal. The chemical shift of the second peak is smaller than that for U(VI) and therefore can be attributed to U(V). The width of the U_3O_8 white line is smaller than that for U_4O_9 and an asymmetry at the higher energy side is notable. We assign the intense structure at ~3726.0 eV to a U(V) contribution. The shoulder at ~3727.5 eV is attributed to U(VI) based on the good correspondence of the position of this feature and that of the hexavalent U reference system. We simulated the experimental data using the Anderson impurity model for the U(IV), U(V), and U(VI) systems (Fig. 3). The observed fairly good agreement between experimental and calculated spectra provides further support for our assignments. The calculations were performed in a similar way as described in Refs. [37,38]. The model parameters used in the calculations [39] are summarized in Table I.

The experimental data collected for U_4O_9 and U_3O_8 show evidence of mixed oxidation states—predominantly U(IV) and U(V) in the spectrum of U_4O_9 and U(V) and U(VI) in the spectrum of U_3O_8. We did not observe a significant U(VI) contribution for U_4O_9 and neither a U(IV) contribution for U_3O_8. The absence of U(IV) in one of the final phases (U_3O_8) of the oxidation process of UO_2 has important consequences. Desgranges and coworkers [19] reported an increase of the distance between two U layers in the crystal structure of U_3O_8 which is responsible for the volume increase [21] during the UO_2-U_3O_8 transformation. We show here that in addition to the volume change, the chemical properties of U_3O_8 may be different than previously expected due to the absence of U(IV). The absence of U(IV) and presence of U(V) in the U_3O_8 phase may explain the recently reported observation of fast chemical reactions [9,10]. At the same time, our data demonstrate that the oxidation reaction of UO_2 progresses through the three oxidation states: U(IV) → U(V) → U(VI). The possibility for a detailed study of the chemical state of U will improve the understanding of the U participation in geochemical processes.

TABLE I. Values for the parameters used in the Anderson impurity model calculations, where κ is a scaling coefficient for the Slater integrals that describe the $3d$–$5f$ and $5f$–$5f$ Coulomb and exchange interactions, Δ is defined as an energy difference between centers of gravity of $5f^{n+1}\underline{L}$ and $5f^n$ configurations, U_{ff} is a Coulomb interaction parameter for $5f$ electrons, U_c is a $3d$ core-hole potential, V_g and V_f represent electron hopping between $5f$ and ligand orbitals due to their hybridization in the ground and final states, respectively. All values except for those for κ are in units of eV.

Parameter	U(VI)	U(V)	U(IV)
κ	0.7	0.7	0.8
Δ	0.5	3.5	6.5
U_{ff}	3.0	3.5	4.0
U_c	5.5	5.5	5.5
V_g	1.0	1.2	1.2
V_f	0.8	0.95	0.95

We have presented a novel approach to directly probe the U $5f$ valence shell by means of high energy resolution x-ray absorption spectroscopy at the U $3d$ edge. Similar measurements on the distribution of the $5f$ electrons can be performed for other actinides and be extended to demanding sample environments such as high pressure and high or low temperature by using the present experimental setup. Here, we find that the transformation of UO_2 to U_3O_8 involves a complex modification of the U oxidation states. The observed oxidation states of mixed-valence U oxides are in disagreement with previous assumptions [20,27]. The results call for a revision of the understanding of the U chemistry in certain chemical reactions and provide new input to the discussion on long-term storage and the ability to recycle the products of spent nuclear fuel.

The authors would like to thank the technical support staff and P. Colomp at the ESRF for the assistance during the experiment. K. O. K. would like to thank S. Conradson for the fruitful discussions, J. Grattage for support, and D. Hudry for providing the $UO_2(acac)_2$ sample. P. M.

acknowledges G. Baldinozzi and L. Desgranges for the synthesis of the U_4O_9 sample.

*kristina.kvashnina@esrf.fr

[1] P. C. Burns, R. C. Ewing, and A. Navrotsky, Science **335**, 1184 (2012).

[2] J. W. L. Pang, W. J. L. Buyers, A. Chernatynskiy, M. D. Lumsden, B. C. Larson, and S. R. Phillpot, Phys. Rev. Lett. **110**, 157401 (2013).

[3] J. G. Tobin and S.-W. Yu, Phys. Rev. Lett. **107**, 167406 (2011).

[4] S. Carretta, P. Santini, R. Caciuffo, and G. Amoretti, Phys. Rev. Lett. **105**, 167201 (2010).

[5] Y. Q. An, A. J. Taylor, S. D. Conradson, S. A. Trugman, T. Durakiewicz, and G. Rodriguez, Phys. Rev. Lett. **106**, 207402 (2011).

[6] Q. Yin and S. Y. Savrasov, Phys. Rev. Lett. **100**, 225504 (2008).

[7] S. L. Dudarev, D. N. Manh, and A. P. Sutton, Philos. Mag. B **75**, 613 (1997).

[8] M. Chollet, R. C. Belin, J.-C. Richaud, M. Reynaud, and F. Adenot, Inorg. Chem. **52**, 2519 (2013).

[9] M. P. Kanouff, P. E. Gharagozloo, M. Salloum, and A. D. Shugard, Chem. Eng. Sci. **91**, 212 (2013).

[10] M. Marchand, O. Fiquet, and M. Brothier, J. Nucl. Mater. **437**, 310 (2013).

[11] T. Nagai, N. Sato, S.-ichi Kitawaki, A. Uehara, T. Fujii, H. Yamana, and M. Myochin, J. Nucl. Mater. **433**, 397 (2013).

[12] G. J. Hutchings, C. S. Heneghan, I. D. Hudson, and S. H. Taylor, Nature (London) **384**, 341 (1996).

[13] D. Kumar and N. M. Gupta, Catal. Surv. Asia **9**, 35 (2005).

[14] D. A. Andersson, G. Baldinozzi, L. Desgranges, D. R. Conradson, and S. D. Conradson, Inorg. Chem. **52**, 2769 (2013).

[15] S. D. Conradson, D. Manara, F. Wastin, D. L. Clark, G. H. Lander, L. A. Morales, J. Rebizant, and V. V. Rondinella, Inorg. Chem. **43**, 6922 (2004).

[16] Y. Yun, J. Rusz, M.-T. Suzuki, and P. M. Oppeneer, Phys. Rev. B **83**, 1 (2011).

[17] J. Y. Colle, J.-P. Hiernaut, D. Papaioannou, C. Ronchi, and A. Sasahara, J. Nucl. Mater. **348**, 229 (2006).

[18] F. Garrido, a C. Hannon, R. M. Ibberson, L. Nowicki, and B. T. M. Willis, Inorg. Chem. **45**, 8408 (2006).

[19] L. Desgranges, G. Baldinozzi, G. Rousseau, J.-C. Nièpce, and G. Calvarin, Inorg. Chem. **48**, 7585 (2009).

[20] S. D. Conradson, B. D. Begg, D. L. Clark, C. den Auwer, M. Ding, P. K. Dorhout, F. J. Espinosa-Faller, P. L. Gordon, R. G. Haire, N. J. Hess, R. F. Hess, D. W. Keogh, G. H. Lander, D. Manara, L. A. Morales, M. P. Neu, P. Paviet-Hartmann, J. Rebizant, V. V. Rondinella, W. Runde, C. D. Tait, D. K. Veirs, P. M. Villella, and F. Wastin, J. Solid State Chem. **178**, 521 (2005).

[21] H. Geng, Y. Chen, Y. Kaneta, M. Iwasawa, T. Ohnuma, and M. Kinoshita, Phys. Rev. B **77**, 104120 (2008).

[22] J. J. Pireaux, J. Riga, E. Thibaut, C. Tenret-Noël, R. Caudano, and J. J. Verbist, Chem. Phys. **22**, 113 (1977).

[23] G. Curran, Y. Sevestre, W. Rattray, P. Allen, and K. Czerwinski, J. Nucl. Mater. **323**, 41 (2003).

[24] E. A. Hudson, J. J. Rehr, and J. J. Bucher, Phys. Rev. B **52**, 13 815 (1995).

[25] S. M. Butorin, *Actinide Nanoparticles Research*, edited by S. N. Kalmykov and M. A. Denecke (Springer Science, New York, 2011), p. 63.

[26] K. Grossmann, T. Arnold, R. Steudtner, S. Weiss, and G. Bernhard, Naturwissenschaften **96**, 963 (2009).

[27] H. Idriss, Surf. Sci. Rep. **65**, 67 (2010).

[28] Y. A. Teterin and A. Y. Teterin, Russ. Chem. Rev. **73**, 541 (2004).

[29] T. Gouder, A. Seibert, L. Havela, and J. Rebizant, Surf. Sci. **601**, L77 (2007).

[30] T. Vitova, K. O. Kvashnina, G. Nocton, G. Sukharina, M. A. Denecke, S. M. Butorin, M. Mazzanti, R. Caciuffo, A. Soldatov, T. Behrends, and H. Geckeis, Phys. Rev. B **82**, 235118 (2010).

[31] M. O. Krause and J. H. Oliver, J. Phys. Chem. Ref. Data **8**, 329 (1979).

[32] J. Petiau, G. Calas, D. Petitmaire, A. Bianconi, M. Benfatto, and A. Marcelli, Phys. Rev. B **34**, 7350 (1986).

[33] S. M. Butorin, J. Electron Spectrosc. Relat. Phenom. **110–111**, 213 (2000).

[34] P. Glatzel, T.-C. Weng, K. Kvashnina, J. Swarbrick, M. Sikora, E. Gallo, N. Smolentsev, and R. A. Mori, J. Electron Spectrosc. Relat. Phenom. **188**, 17 (2013).

[35] J. C. Swarbrick, U. Skyllberg, T. Karlsson, and P. Glatzel, Inorg. Chem. **48**, 10 748 (2009).

[36] C. Gauthier, V. A. Solé, R. Signorato, J. Goulon, and E. Moguiline, J. Synchrotron Radiat. **6**, 164 (1999).

[37] S. M. Butorin, D. C. Mancini, J.-H. Guo, N. Wassdahl, J. Nordgren, M. Nakazawa, S. Tanaka, T. Uozumi, A. Kotani, Y. Ma, K. Myano, B. Karlin, and D. Shuh, Phys. Rev. Lett. **77**, 574 (1996).

[38] M. Nakazawa, H. Ogasawara, and A. Kotani, Surf. Rev. Lett. **09**, 1149 (2002).

[39] The ground state of the uranium systems was represented by a linear combination of the $5f^n$, $5f^{n+1}\underline{L}$, and $5f^{n+2}\underline{L}^2$ ($\underline{L}$ stands for a hole in the ligand $2p$ band) electronic configurations with $n = 2$ for U(IV), $n = 1$ for U(V), and $n = 0$ for U(VI) ions, respectively. The final state of the spectroscopic process was described as a linear combination of $3d^95f^{n+1}$, $3d^95f^{n+2}\underline{L}$, and $3d^95f^{n+3}\underline{L}^2$ configurations. The full multiplet structure due to $3d$–$5f$ and $5f$–$5f$ Coulomb, exchange, and spin-orbit interactions was also taken into account (note that for U(IV) and U(V), only the first two electronic configurations were included in the calculations for the ground and final state because the contribution of the third configuration is expected to be small). The spectra were calculated by obtaining the transition matrix elements from a chain of the modified programs from the TT-MULTIPLETS package, http://www.esrf.eu/computing/scientific/exafs/tt-multiplets.html.